Métodos de RMN no estado sólido

Jair C. C. Freitas

Programa de Pós-graduação em Física – UFES

Programa de Pós-graduação em Química - UFES

Sumário

- Técnicas de alta resolução em RMN de sólidos:
  - Alargamento por anisotropia das interações de spin nuclear em sólidos.
  - Rotação em torno do ângulo mágico (MAS).
  - Ecos rotacionais e bandas laterais.
  - Instrumentação para MAS.
  - Exemplos.

Interações de spin nuclear: resumo

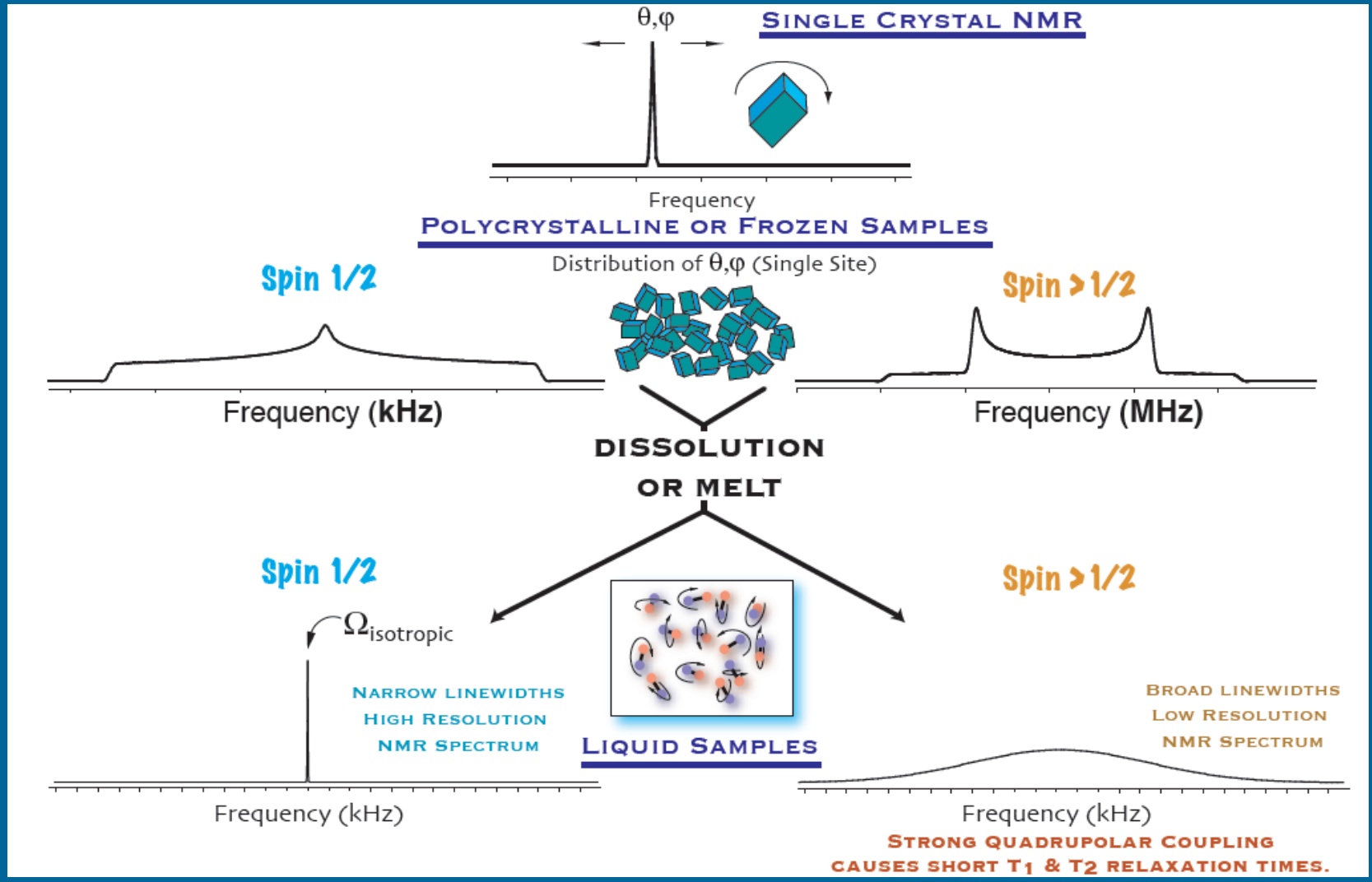

http://grandinetti.org/Research/NMRMethods/index.html

RMN em sólidos policristalinos

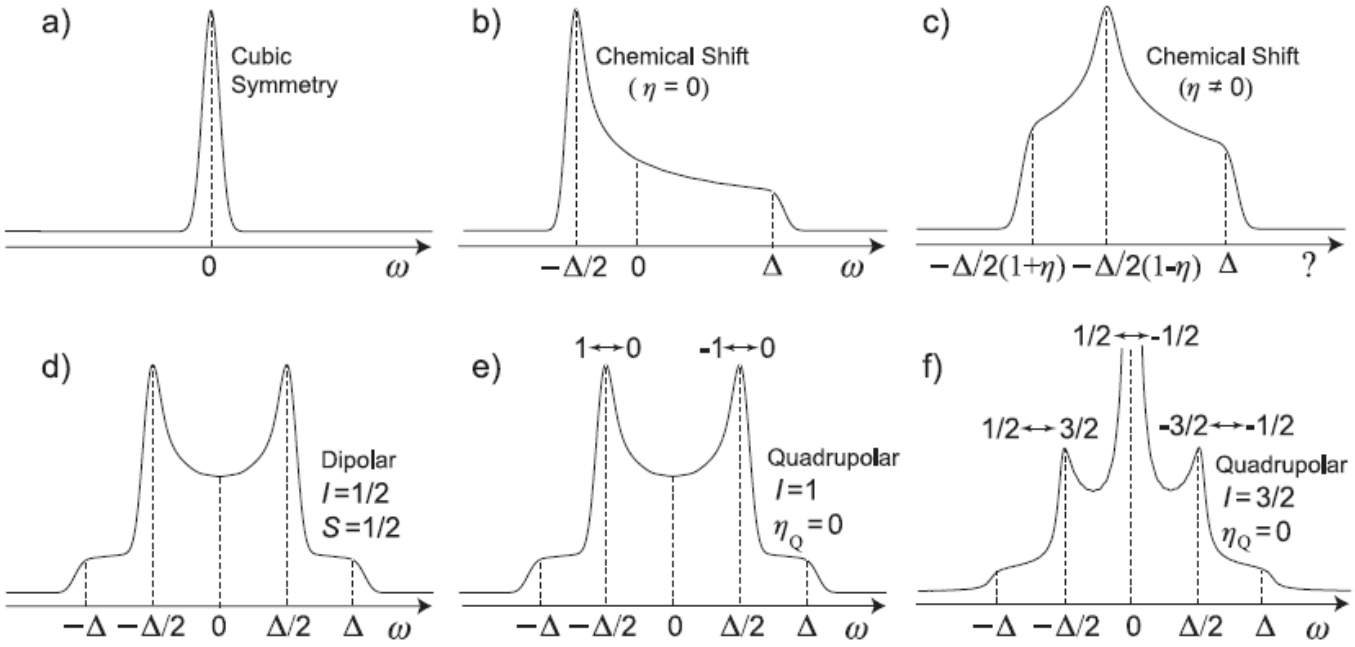

Figure 2.8 Typical powder-pattern spectra observed in polycrystalline solids: Chemical Shift under (a) cubic, (b) axial, and (c) non-axial symmetries; (d) Dipolar interaction between two spins 1/2 (I and S); Quadrupolar interaction for spins e) 1 and f) 3/2, considering an EFG with axial symmetry. The zero of the frequency scale in each case corresponds to the frequency associated with isotropic average (as occurring in liquids). The parameter Δ depends on the anisotropy of the tensors describing each of the interactions.

"NMR Quantum Information Processing", Oliveira et al. Elsevier, 2007.

Anisotropia de deslocamento químico

Frequência dependente da orientação molecular:

$$\omega(\theta,\phi) = \omega_L - \omega_L \left\{ \sigma_{iso} + \frac{\zeta}{2}\left[(3\cos^2\theta - 1) + \eta \,\mathrm{sen}^2\theta \cos 2\phi \right] \right\}$$

Monocristal

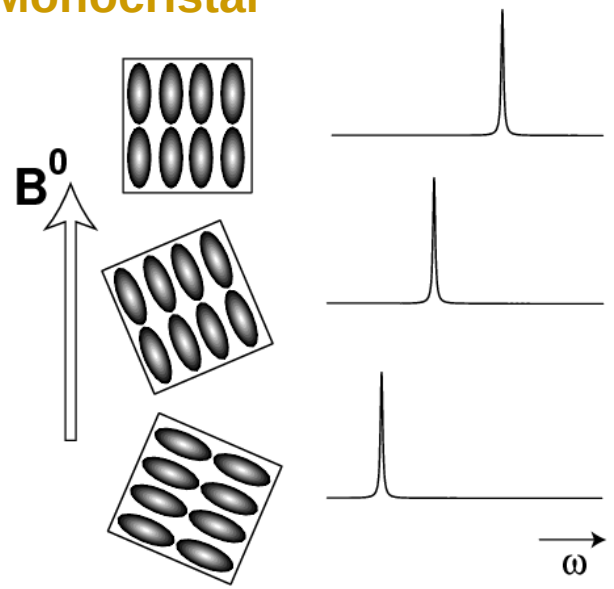

Sólido policristalino ou pó

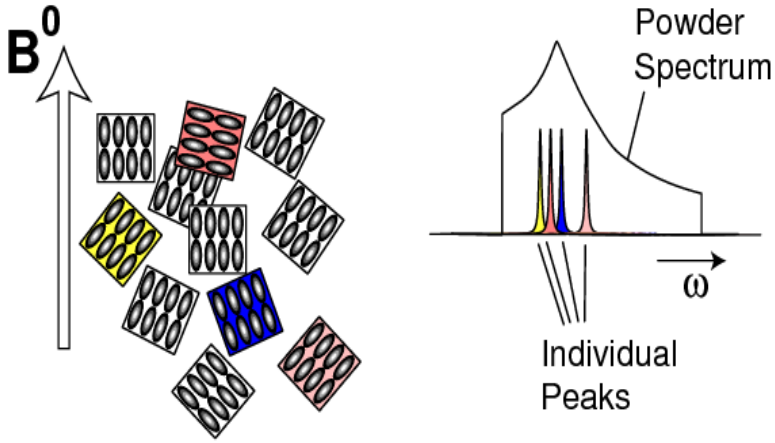

"Spin dynamics", M. H. Levitt. John Wiley & Sons, 2002.

Interação dipolar internuclear

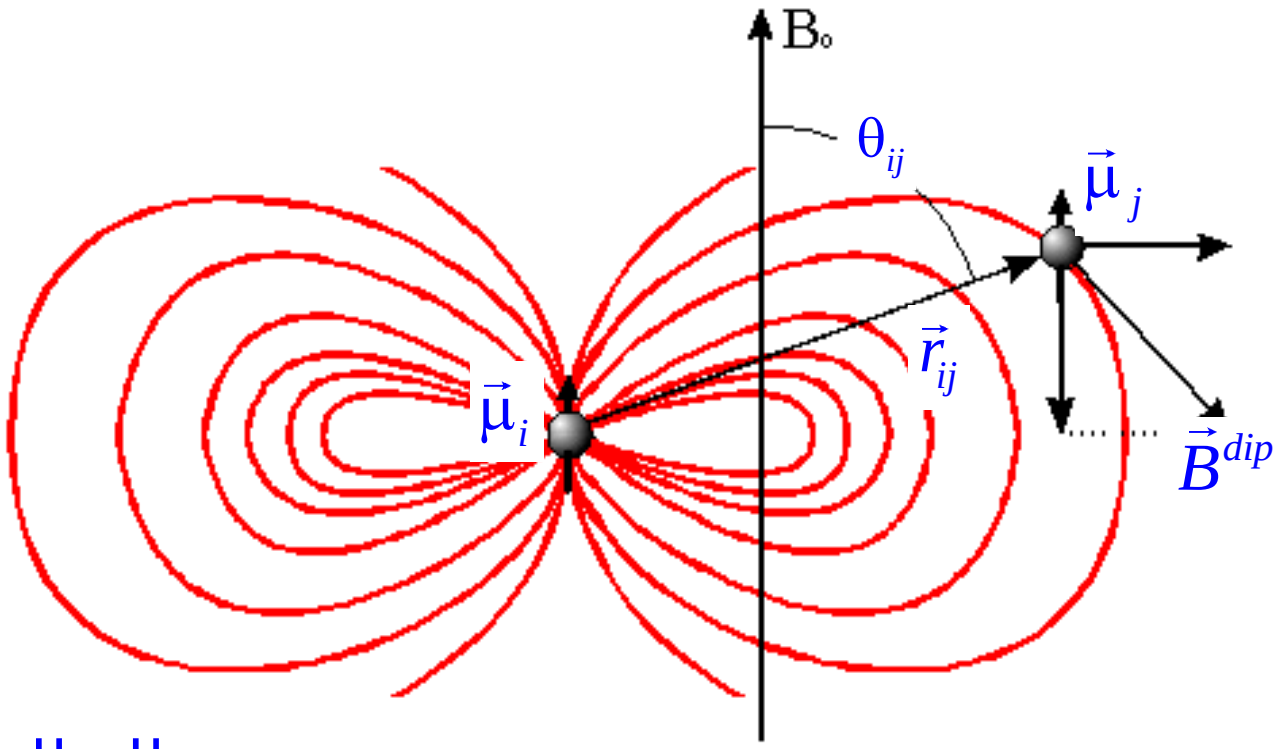

$$B_z^{dip} \cong \frac{\mu_0}{4\pi}\frac{\mu}{r_{ij}^3}(3\cos^2\theta_{ij} - 1)$$

Interação através do espaço

Interação quadrupolar elétrica

Correções de primeira e segunda ordens – caso de simetria axial:

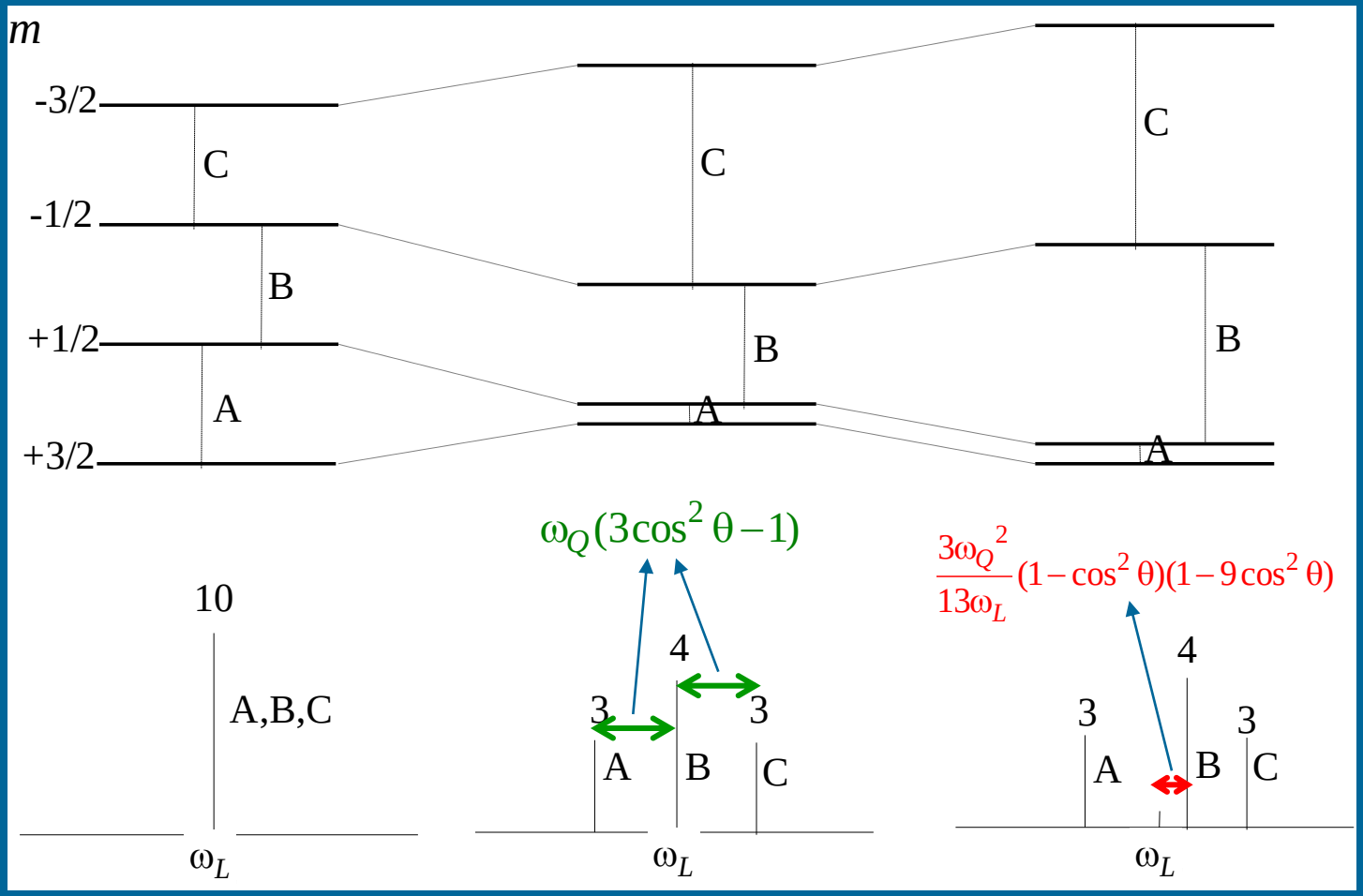

$I = 3/2$

$\eta_Q = 0$

Rotação em torno do ângulo mágico (MAS)

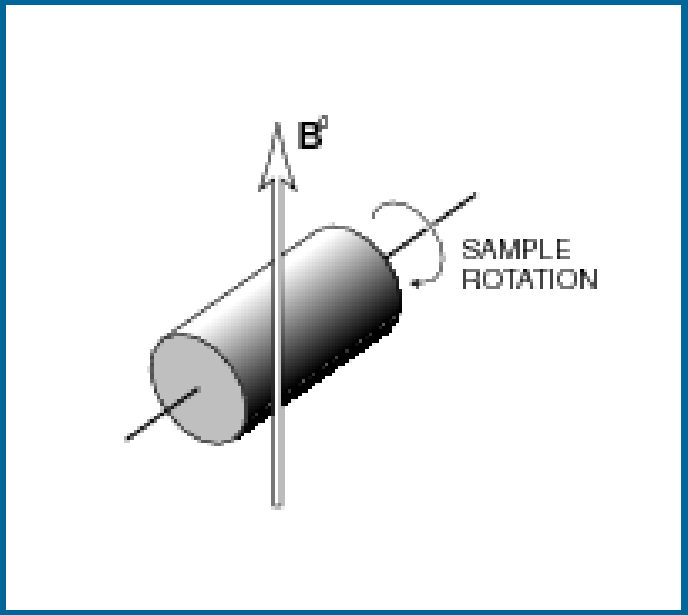

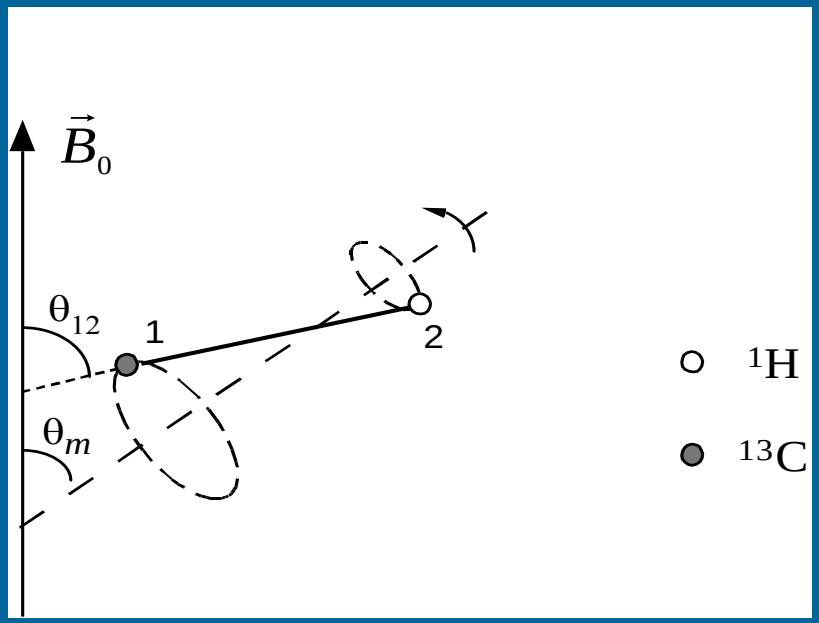

$$\left\langle 3\cos^2\theta_{12} - 1 \right\rangle \propto 3\cos^2\theta_m - 1 = 0$$

$$\theta_m = \cos^{-1}(1/\sqrt{3}) = 54{,}74^o$$

Andrew, Nature 1958;182:1659.
Lowe, Phys. Rev. Lett. 1959;2:285.

Rotação em torno do ângulo mágico (MAS)

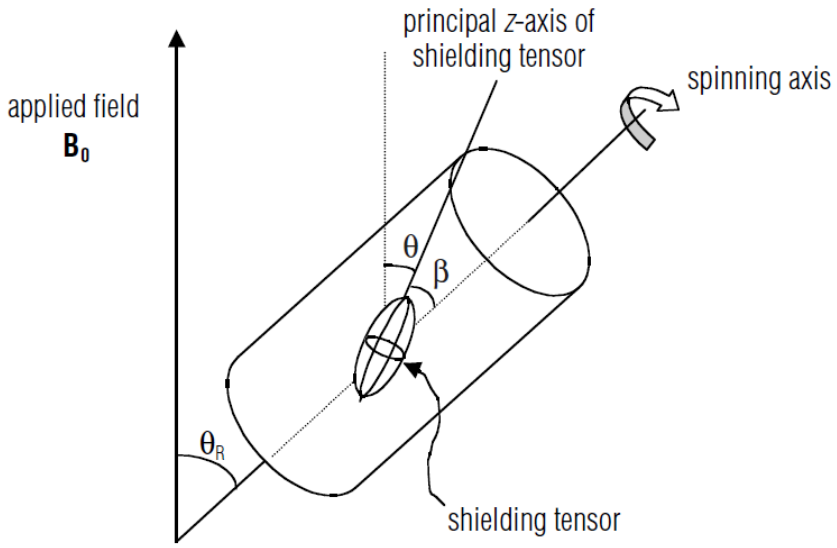

Fig. 2.1 The magic-angle spinning experiment. The sample is spun rapidly in a cylindrical *rotor* about a spinning axis oriented at the magic angle ($\beta = 54.74°$) with respect to the applied magnetic field $\mathbf{B}_0$. Magic-angle spinning removes the effects of chemical shielding anisotropy and heteronuclear dipolar coupling. The chemical shielding tensor is represented here by an ellipsoid; it is fixed in the molecule to which it applies and so rotates with the sample. The angle θ is the angle between $\mathbf{B}_0$ and the principal *z*-axis of the shielding tensor; χ is the angle between the *z*-axis of the shielding tensor principal axis frame and the spinning axis.

$$\langle 3\cos^2\theta - 1\rangle = \frac{1}{2}(3\cos^2\theta_R - 1)(3\cos^2\beta - 1)$$

"Introduction to solid-state NMR spectroscopy", M. J. Duer. Blackwell, 2004.

Rotação em torno do ângulo mágico (MAS)

RMN de ^{19}F – teflon:

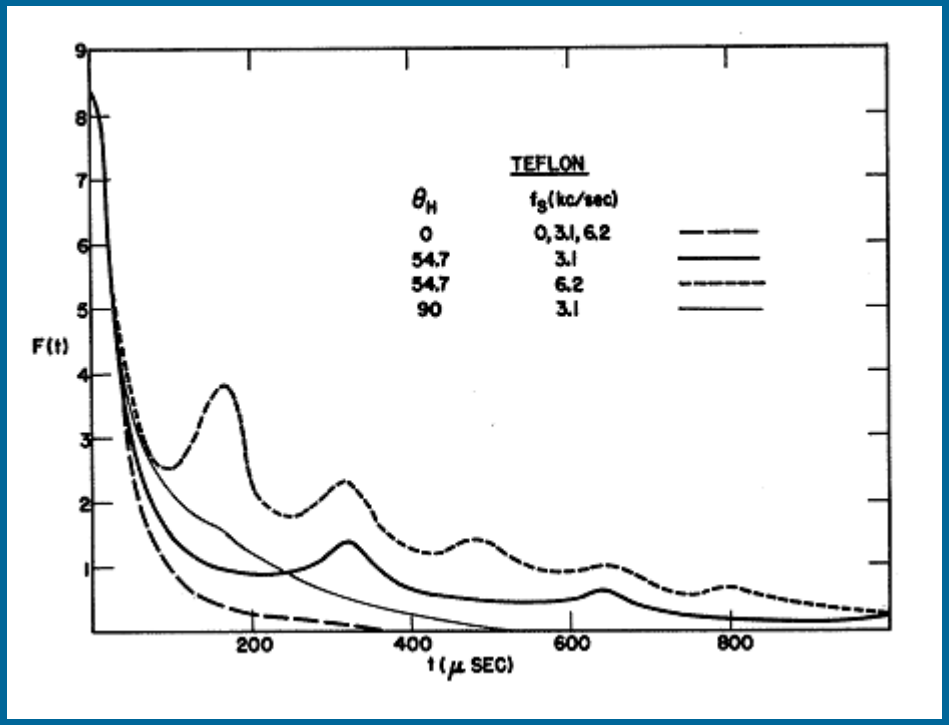

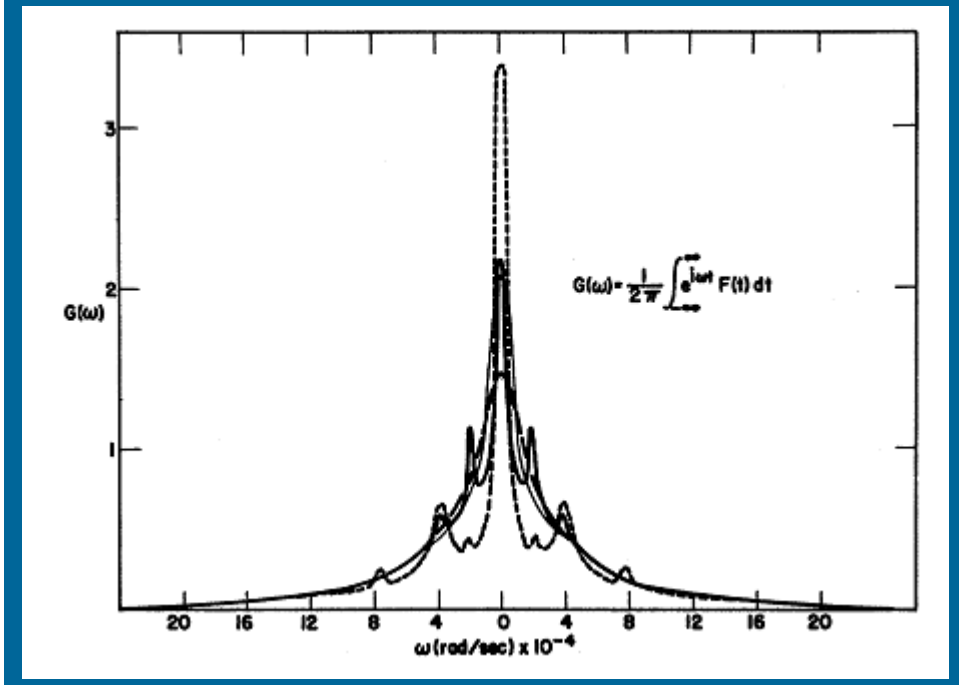

Lowe, Phys. Rev. Lett. 1959;2:285

Rotação em torno do ângulo mágico (MAS)

RMN de ^{13}C (glicina)

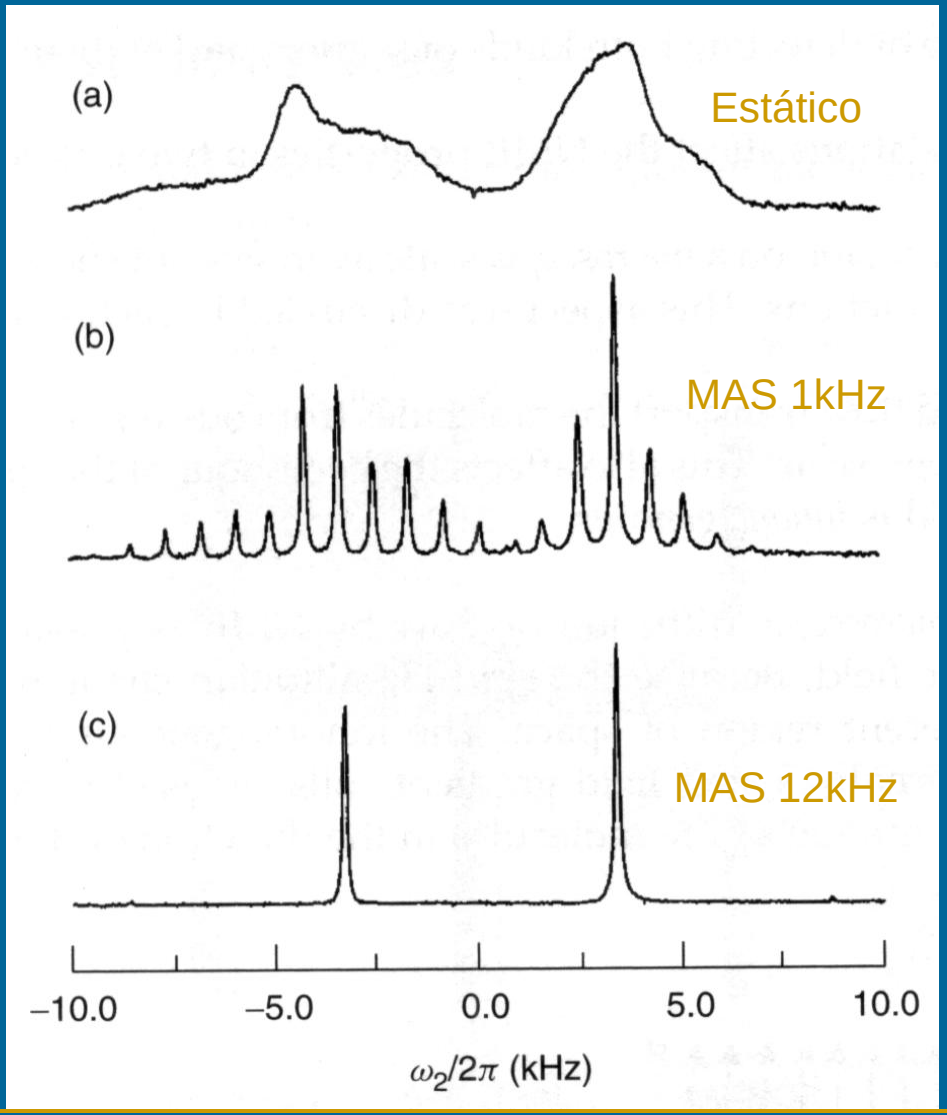

Rotação em torno do ângulo mágico (MAS)

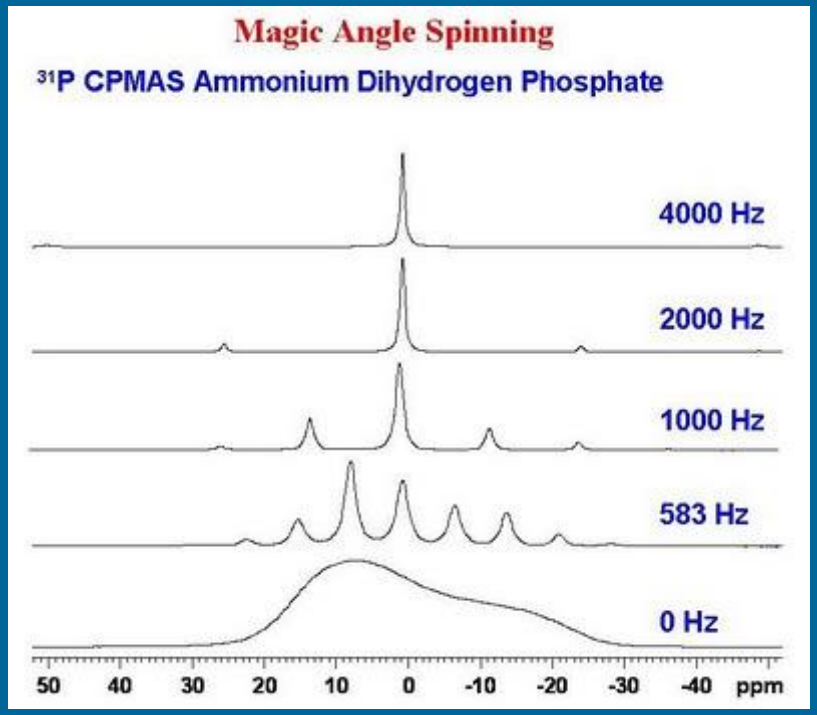

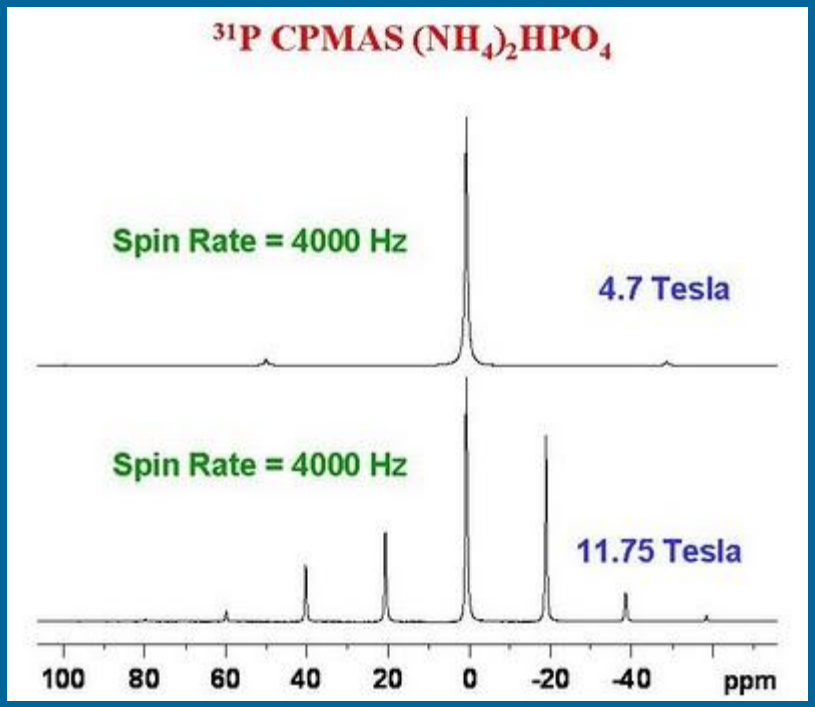

http://u-of-o-nmr-facility.blogspot.com/

Ecos rotacionais e bandas laterais (ssb)

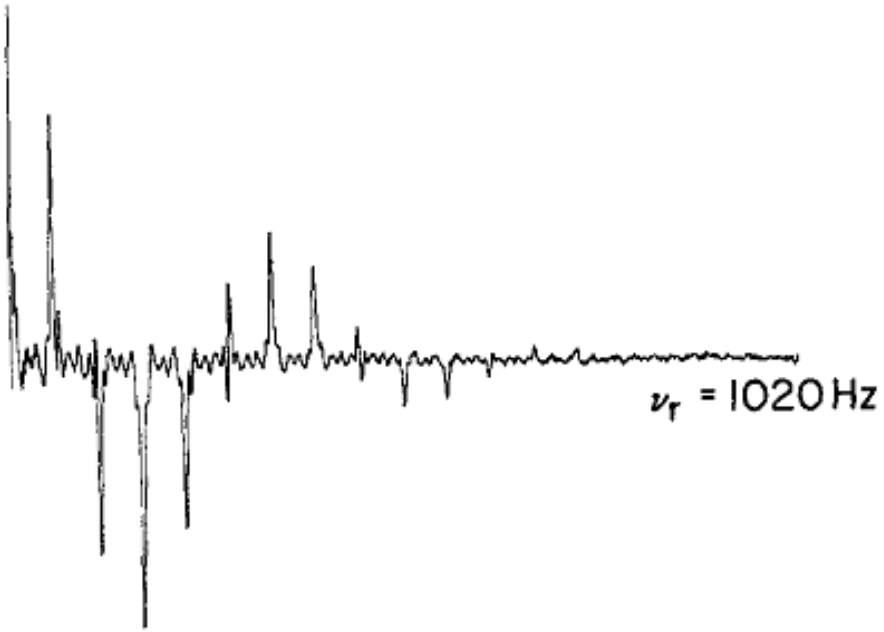

FIG. 1. FID of ^{31}P in powdered barium diethyl phosphate, spinning at $\nu_r = 1020$ Hz. The FID takes the form of a train of rotational spin echoes, spaced by $1/\omega_r = 0.98$ msec. The echo envelope shows an oscillation of period 6.0 msec, because the isotropic chemical shift is off the spectrometer reference frequency by 167 Hz.

Maricq & Waugh, J. Chem. Phys. 1979;70:3300

Ecos rotacionais e bandas laterais (ssb)

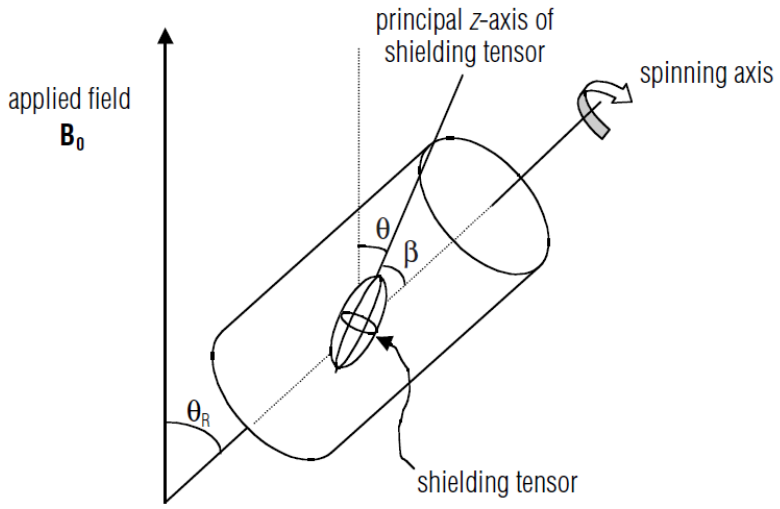

Fig. 2.1 The magic-angle spinning experiment. The sample is spun rapidly in a cylindrical *rotor* about a spinning axis oriented at the magic angle (β = 54.74°) with respect to the applied magnetic field B_0. Magic-angle spinning removes the effects of chemical shielding anisotropy and heteronuclear dipolar coupling. The chemical shielding tensor is represented here by an ellipsoid; it is fixed in the molecule to which it applies and so rotates with the sample. The angle θ is the angle between B_0 and the principal *z*-axis of the shielding tensor; χ is the angle between the *z*-axis of the shielding tensor principal axis frame and the spinning axis.

Anisotropia do deslocamento químico:

$$\omega = -\omega_0 \Big\{ \sigma_{iso} + \frac{1}{2}(3\cos^2\theta_R - 1)(\sigma_{zz}^R - \sigma_{iso}) + \sin^2\theta_R \Big[\frac{1}{2}(\sigma_{xx}^R - \sigma_{yy}^R)\cos(2\omega_R t) + \sigma_{xy}^R \sin(2\omega_R t) \Big] + 2\sin\theta_R \cos\theta_R [\sigma_{xz}^R \cos(\omega_R t) + \sigma_{yz}^R \sin(\omega_R t)] \Big\}$$

"Introduction to solid-state NMR spectroscopy", M. J. Duer. Blackwell, 2004.

Ecos rotacionais e bandas laterais (ssb)

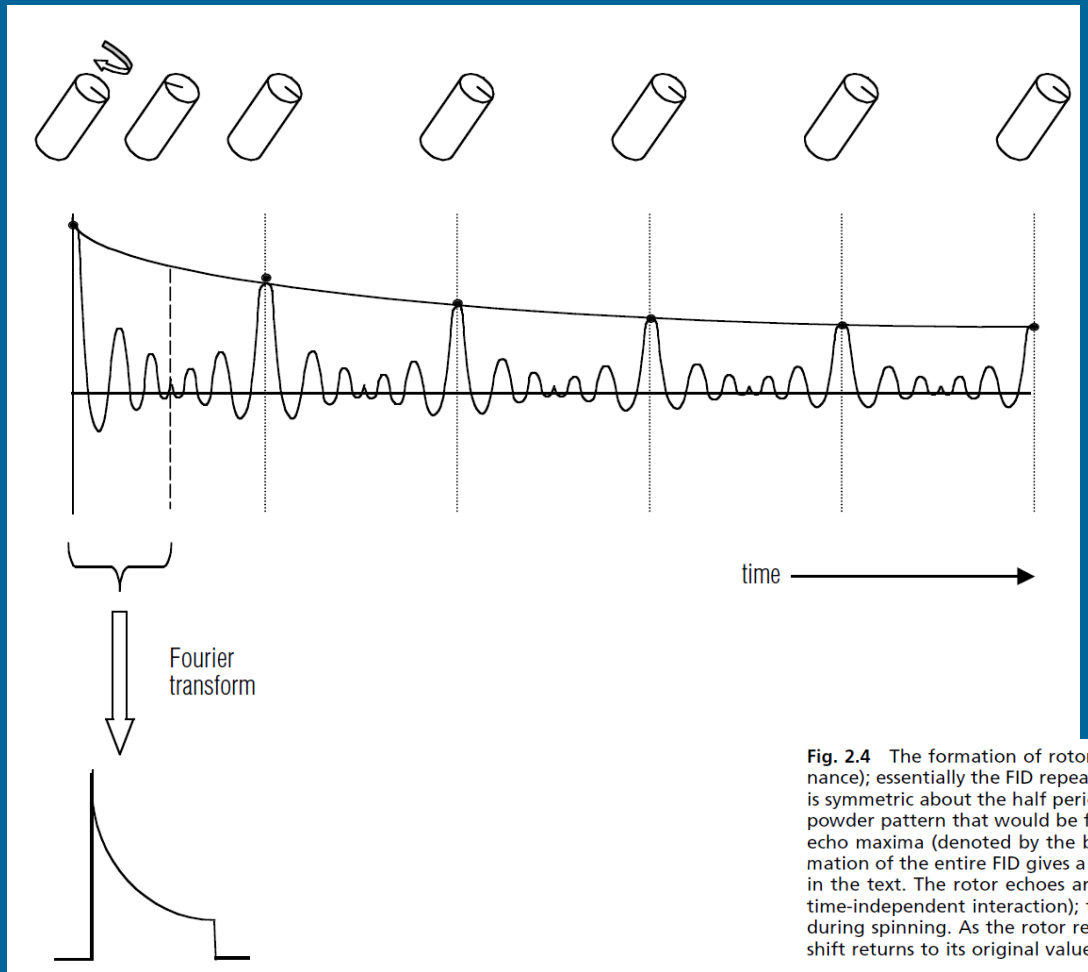

Fig. 2.4 The formation of rotor echoes. The FID shown is that formed under magic-angle spinning (on resonance); essentially the FID repeats every rotor period (marked with dotted lines) and within each rotor period, is symmetric about the half period point. Fourier transformation of one half of a single rotor period gives the powder pattern that would be formed in the absence of magic-angle spinning. Fourier transformation of the echo maxima (denoted by the black dots) gives a single line at the isotropic chemical shift. Fourier transformation of the entire FID gives a line at the isotropic chemical shift flanked by spinning sidebands as described in the text. The rotor echoes arise as a result of the orientation dependence of the chemical shift (or other time-independent interaction); the chemical shift of a given crystallite changes as the rotor changes position during spinning. As the rotor returns to its original position at the end of each rotor period, so the chemical shift returns to its original value and an echo forms in the FID.

"Introduction to solid-state NMR spectroscopy", M. J. Duer. Blackwell, 2004.

Ecos rotacionais e bandas laterais (ssb)

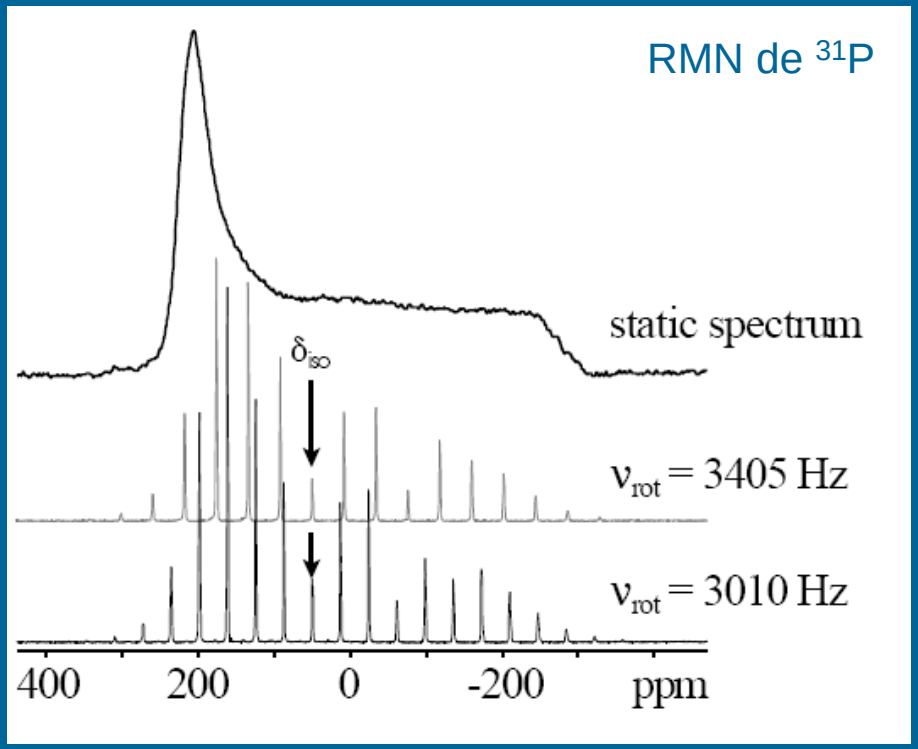

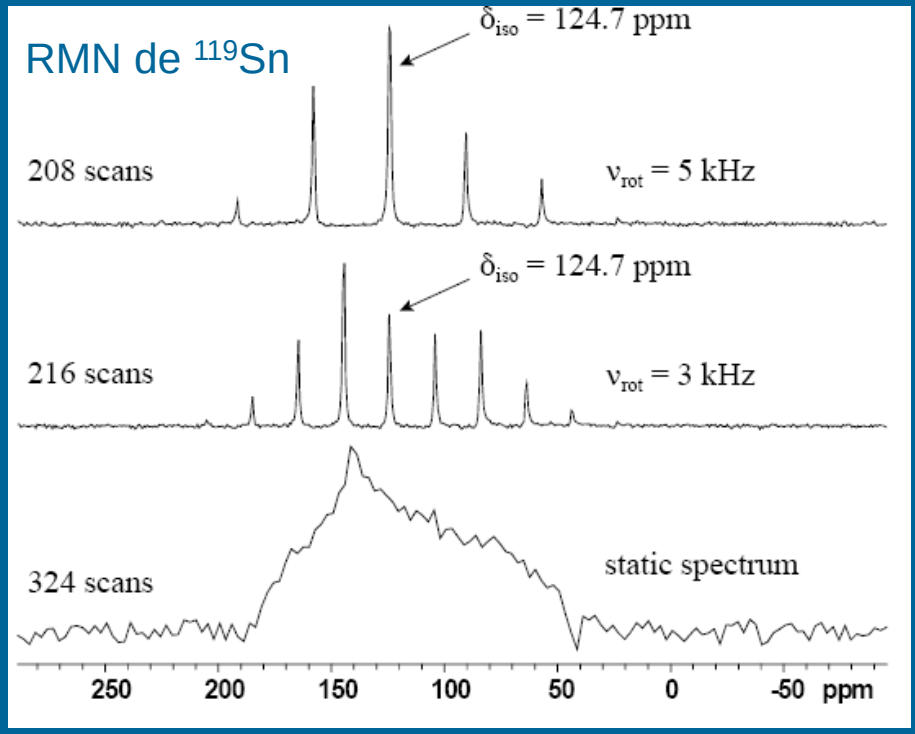

Remoção das bandas laterais: altas frequências de rotação ou técnicas especiais (TOSS).

Supressão de bandas laterais (TOSS)

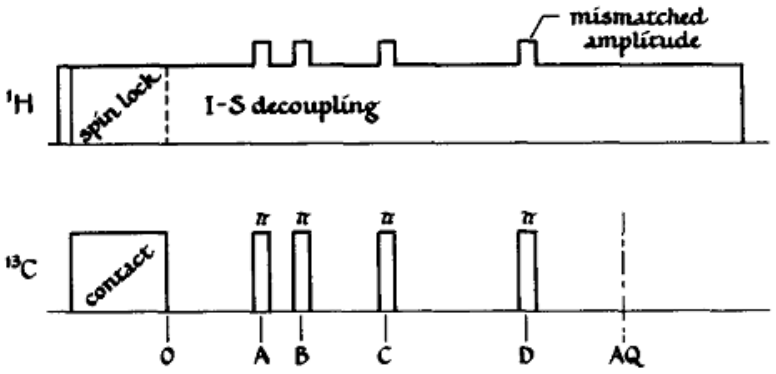

FIG. 10. Pulse sequence which produces spin echoes at arbitrary times in rotating solids. For times A, B, C, D, and AQ see Table II.

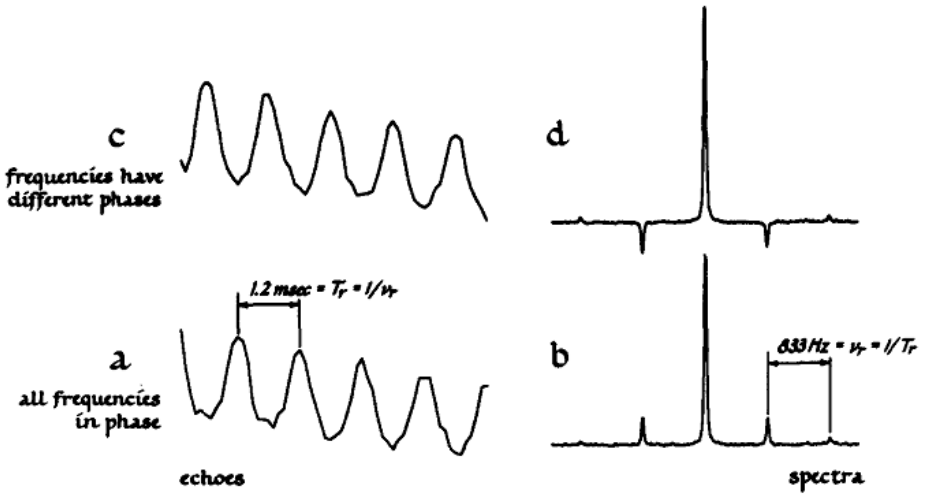

FIG. 2. Echoes and spectra: (a) Beginning of an ordinary fid; (b) Fourier transform of a; (c) Beginning of a train of supplementary echoes; (d) Transform of c.

Dixon, J. Chem . Phys. 1982;77:1800.

Supressão de bandas laterais (TOSS)

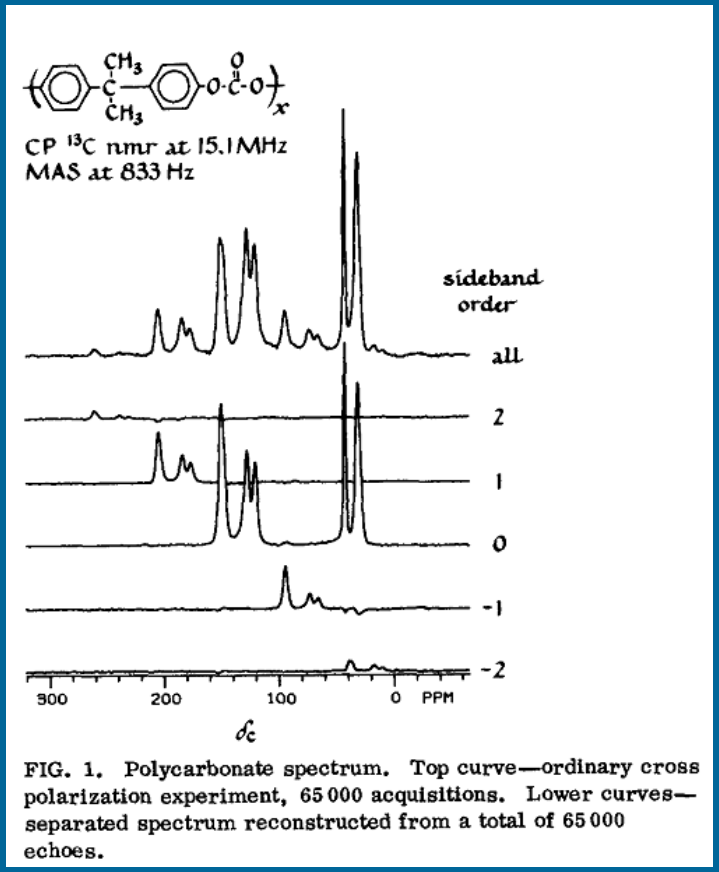

FIG. 1. Polycarbonate spectrum. Top curve—ordinary cross polarization experiment, 65 000 acquisitions. Lower curves—separated spectrum reconstructed from a total of 65 000 echoes.

Dixon, J. Chem . Phys. 1982;77:1800.

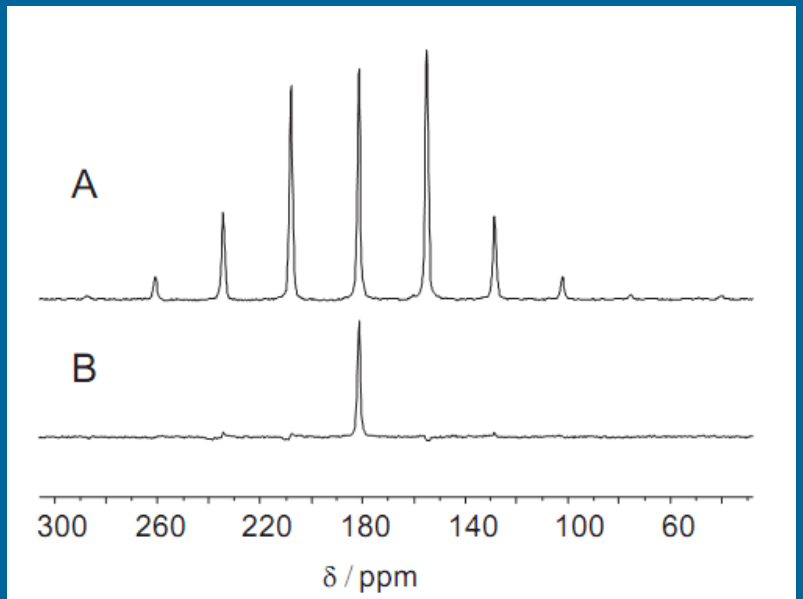

Figure 9: Carbon-13 CP/MAS spectra of singly-labelled (99%) phenylacetic-*carboxy*-^{13}C acid (B_0 = 4.7 T, ν_L = 50.3 MHz, ν_{rot} = 1.339 kHz) acquired with high-power proton decoupling. In spectrum A, a standard CP pulse program was used. The isotropic peak is at 181 ppm. In spectrum B, the TOSS sequence has been used to suppress the spinning sidebands; only the isotropic peak remains. One drawback of the TOSS sequence is the loss of intensity relative to the standard CP/MAS spectrum. Number of acquisitions: 64 (trace A); 128 (trace B).

Bryce et al., Can. J. Anal. Sci. Spectr. 2001;46:46.

Ecos rotacionais e bandas laterais (ssb)

Ajuste do ângulo mágico:

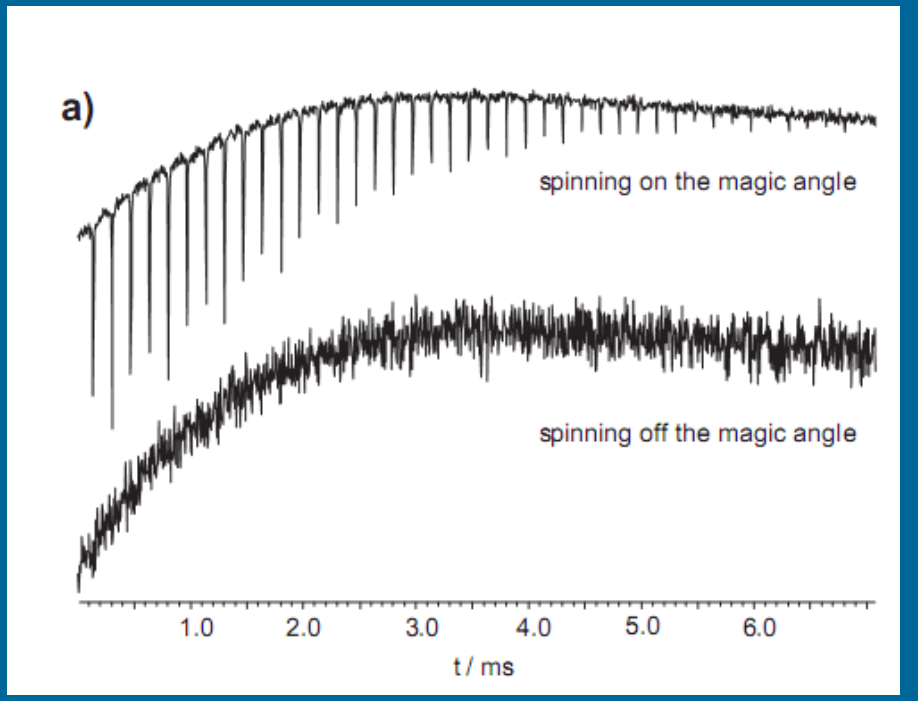

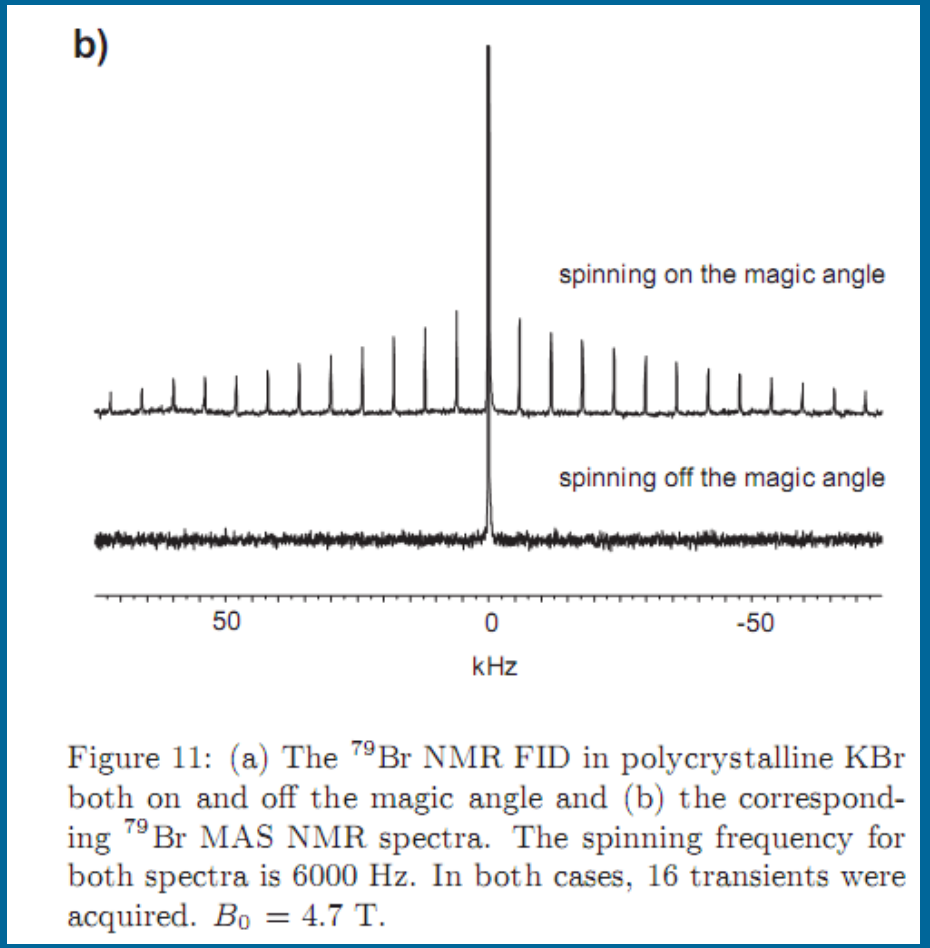

Figure 11: (a) The ^{79}Br NMR FID in polycrystalline KBr both on and off the magic angle and (b) the corresponding ^{79}Br MAS NMR spectra. The spinning frequency for both spectra is 6000 Hz. In both cases, 16 transients were acquired. $B_0 = 4.7$ T.

Bryce et al., Can. J. Anal. Sci. Spectr. 2001;46:46.

Ecos rotacionais e bandas laterais (ssb)

Ajuste do ângulo mágico:

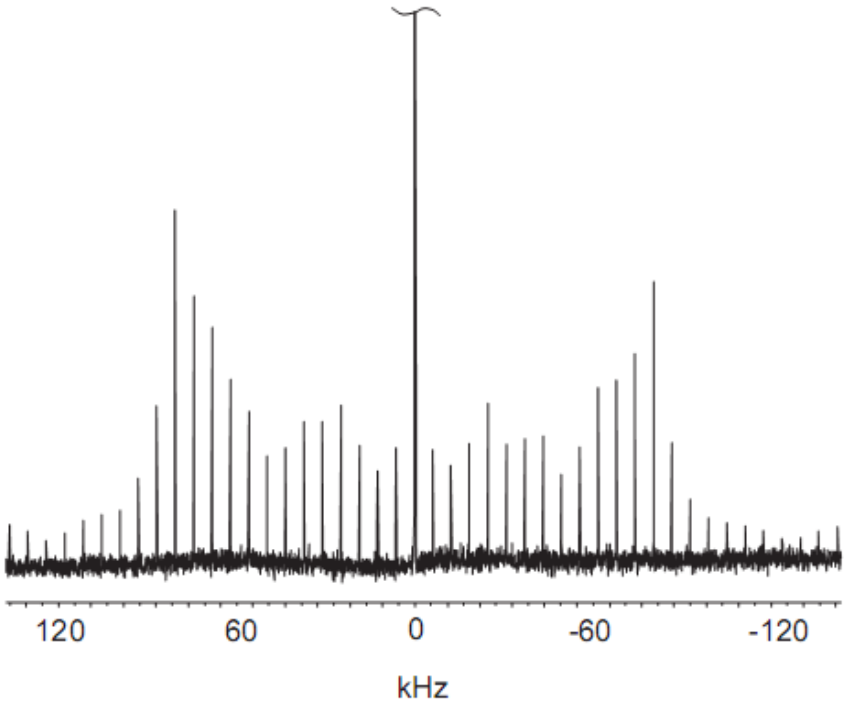

Figure 12: The ^{23}Na NMR spectrum of $NaNO_3$ acquired with sample spinning at the magic angle (spinning rate of 6012 Hz, 16 transients). $B_0 = 4.7$ T.

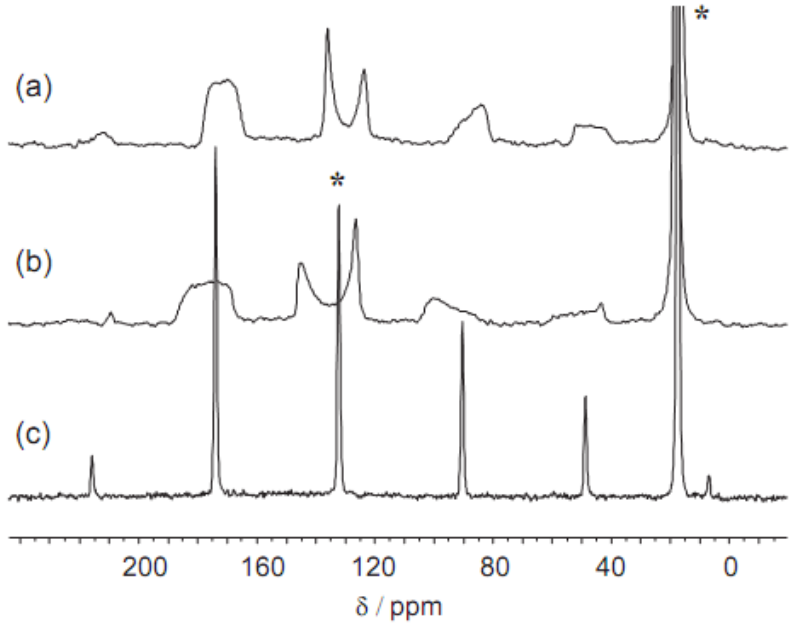

Figure 13: Carbon-13 CP NMR spectra of hexamethylbenzene, with $B_0 = 4.7$ T and the sample spinning at (a) greater than the magic angle and (b) less than the magic angle, and (c) at the magic angle. In all cases, 512 transients were acquired with the sample spinning at 2100 Hz. The isotropic peaks are marked with asterisks. The large peak on the right is due to the methyl carbons.

Bryce et al., Can. J. Anal. Sci. Spectr. 2001;46:46.

Ecos rotacionais e bandas laterais (ssb)

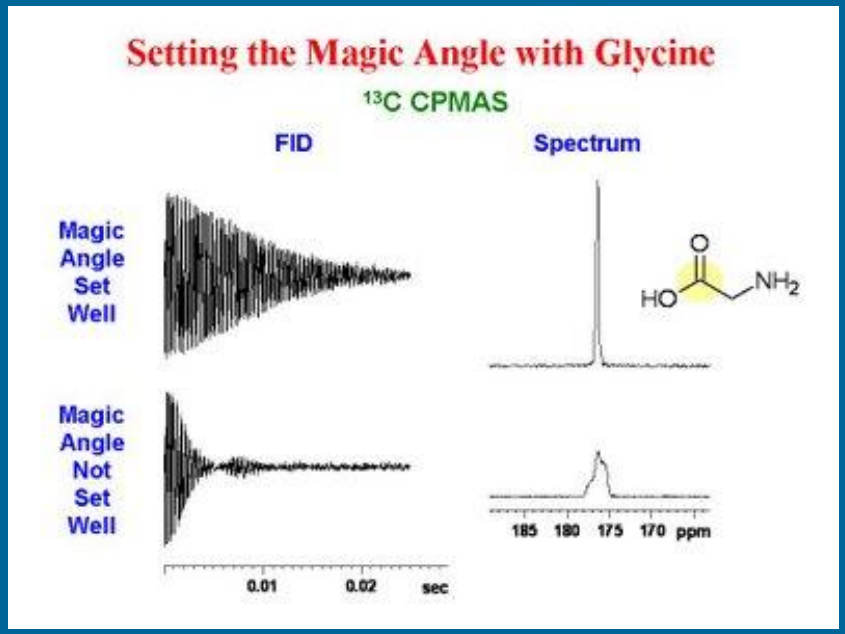

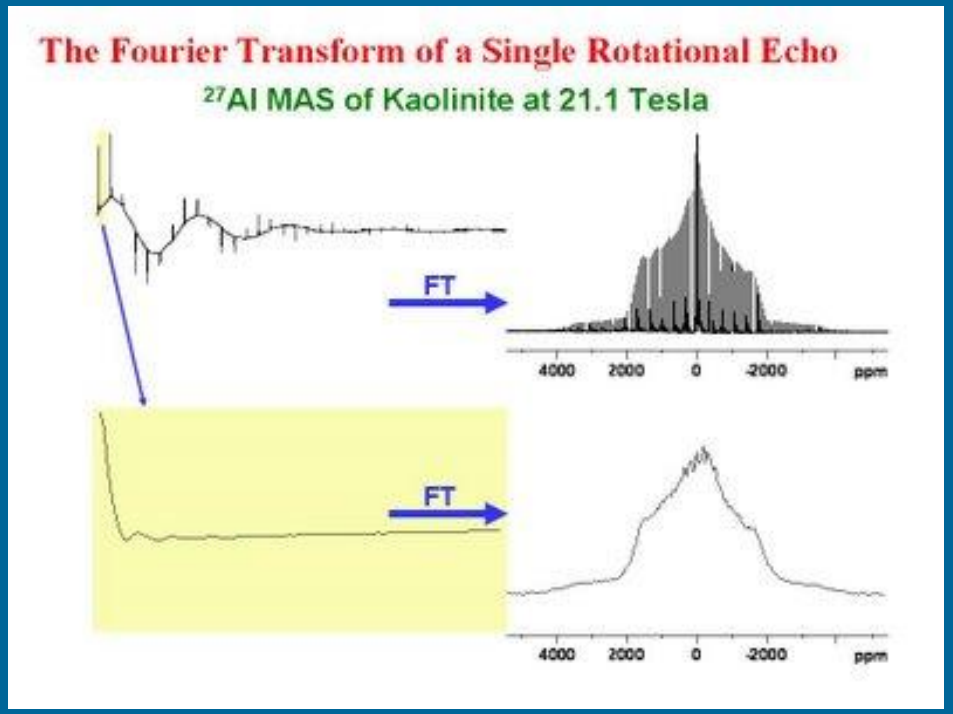

http://u-of-o-nmr-facility.blogspot.com/

MAS e efeitos de CSA: importância da magnitude de B_0

RMN de ^{13}C – simulações com CSA para planos grafenos:

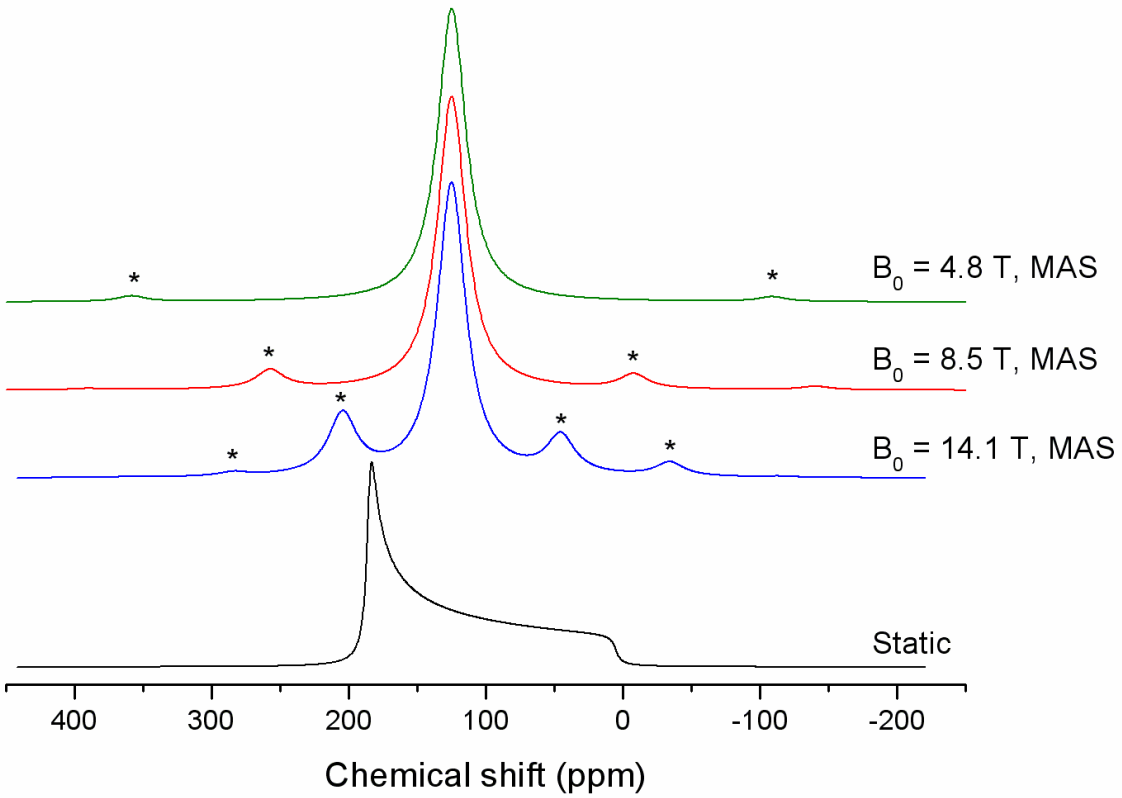

MAS e efeitos de CSA: importância da magnitude de B_0

RMN de ^{13}C – espectros com MAS para materiais carbonizados:

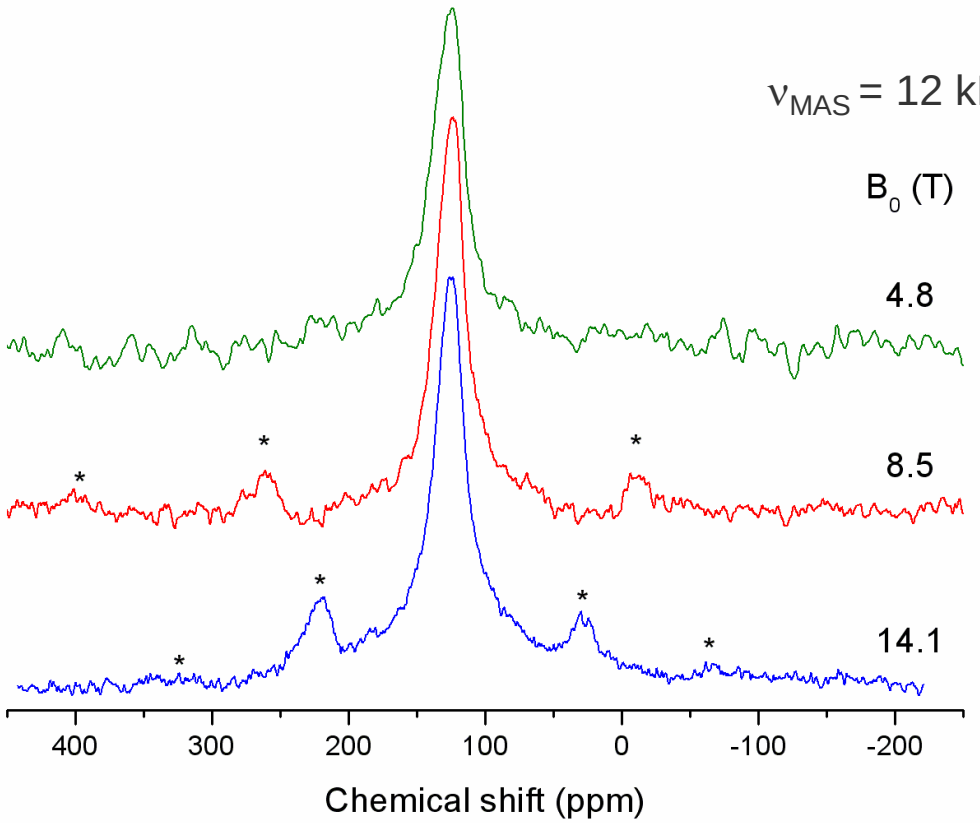

MAS e efeitos de CSA: importância da magnitude de B_0

Magnetic field (T)	^{1}H NMR frequency (MHz)	^{13}C NMR frequency (MHz)	Δf_{CSA} (kHz)
2.35	100	25.2	5
4.70	200	50.3	10
7.05	300	75.4	15
9.39	400	100.6	20
11.74	500	125.8	25
14.09	600	150.9	30
16.44	700	176.1	35
18.79	800	201.2	40
21.14	900	226.4	45

Probes e rotores para experimentos com MAS

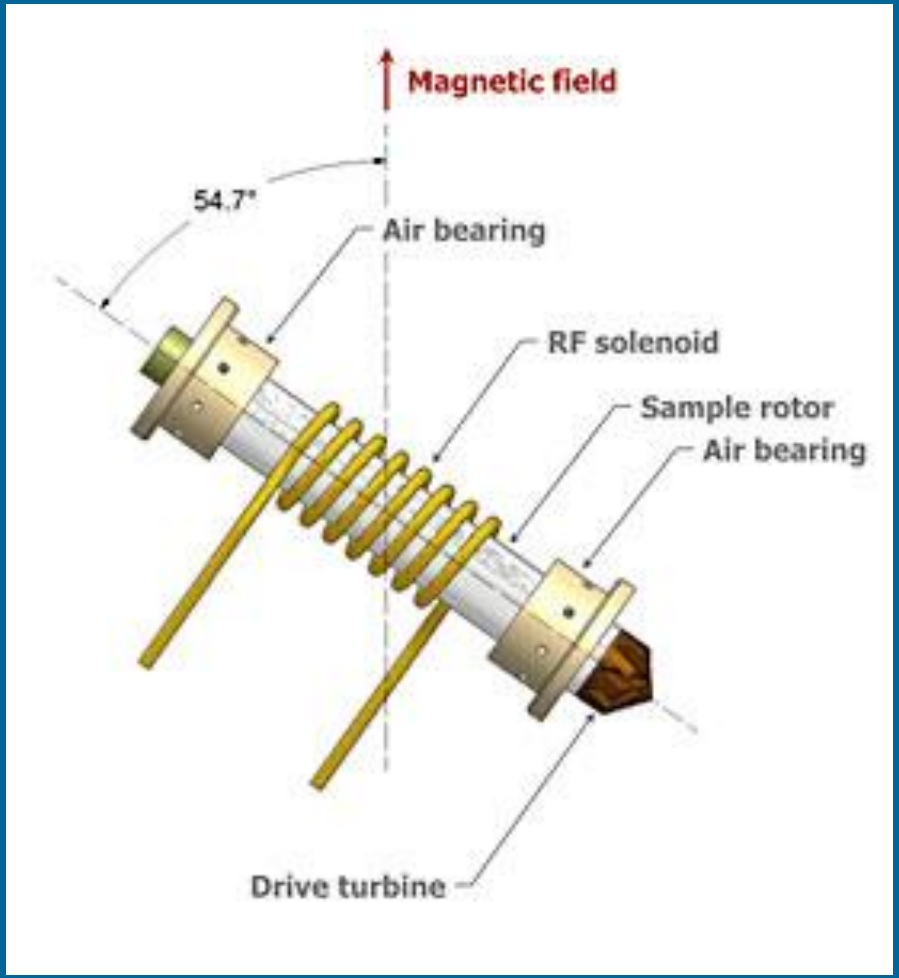

http://www.magnet.fsu.edu/education/tutorials/tools/probes/magicangle.html

Probes e rotores para experimentos com MAS

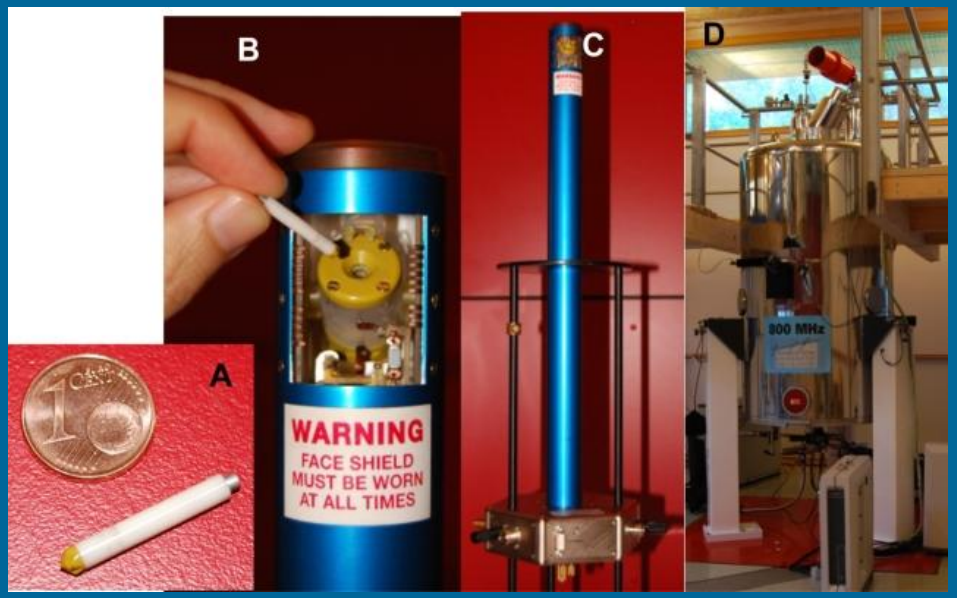

- Rotores menores:
  - ✓ Frequências de MAS maiores.
    - 7mm: f_{MAS} < 8 kHz.
    - 2,5mm: f_{MAS} < 35 kHz.
  - ✓ Menor sensibilidade.

RMN no estado sólido: probes e rotores

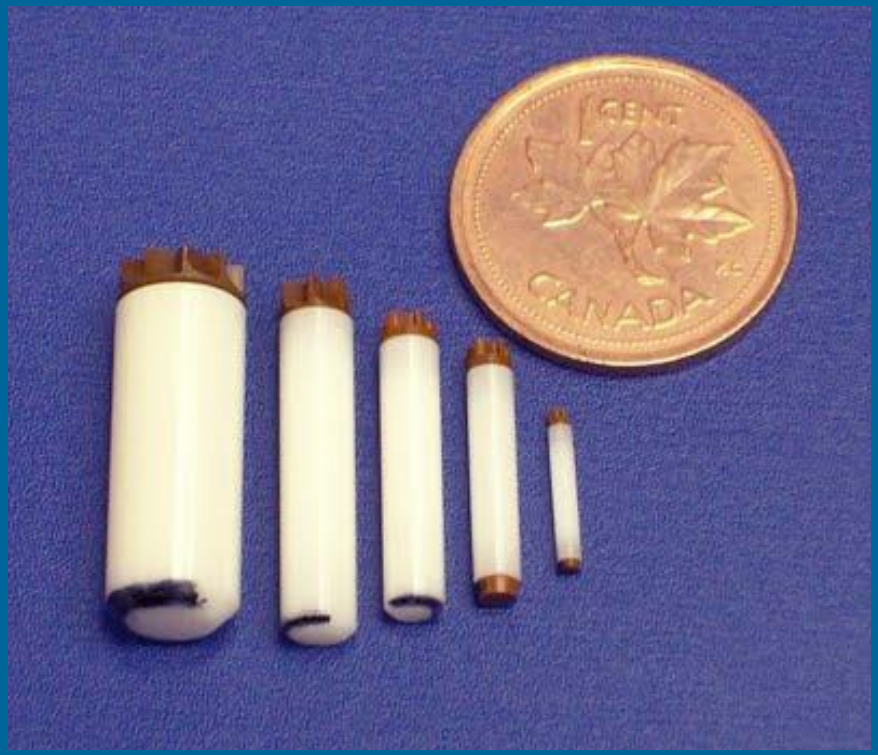

ϕ (mm): 7,0 4,0 3,2 2,5 1,3

$\nu_{rot}^{máx.}$ (kHz): 8 18 23 35 70

http://u-of-o-nmr-facility.blogspot.com/2008/04/how-much-sample-do-i-need-to-get-solid.html

Bibliografia recomendada

- RMN de alta resolução em sólidos:
  - "Multinuclear solid-state NMR of inorganic materials", K. J. D. Mackenzie, M. E. Smith. Pergamon, 2002.
  - "High resolution NMR in solids", U. Haeberlen. In: *Adv. Magn. Reson. Suppl. I*, Academic Press, 1976.
  - "Introduction to solid-state NMR spectroscopy", M. J. Duer. Blackwell, 2004.
  - "NMR in rotating solids", M. M. Maricq, J. S. Waugh. *J. Chem. Phys.* 1979;70:3300-3316.
  - "Practical aspects of modern routine solid-state nuclear magnetic resonance spectroscopy: one-dimensional experiments", D. L. Bryce et al., *Can. J. Anal. Sci. Spectr.* 2001;46:46.
  - "Recent advances in experimental solid state NMR methodology for half-integer spin quadrupolar nuclei", M. E. Smith, E. R. H. van Eck. *Prog. Nucl. Magn. Reson. Spectr.* 1999;34:159-201.